International Journal of Psychophysiology 226 (2026) 113422

Contents lists available at ScienceDirect

International Journal of Psychophysiology

journal homepage: www.elsevier.com/locate/ijpsycho

Pupil behaviour across contexts: from resting oscillations to social reactivity

Vivien Rabadan [a], Camille Ricou [a], Yassine Mofid [a], Nadia Aguillon-Hernandez [a], Claire Wardak [a,*]

[a] Université de Tours, INSERM, Imaging Brain & Neuropsychiatry iBraiN U1253, 37032, Tours, France

ARTICLE INFO

Keywords:
Pupillometry
Pupillary light reflex
Hippus
Arousal
Faces

ABSTRACT

Pupil diameter is shaped by central arousal mechanisms, autonomic drive and the biomechanical constraints of the iris. Although tonic pupil size is often treated as an index of baseline arousal, pupillary dynamics reflect partially dissociable physiological axes. We aimed to characterise this network organisation in a group of young adults and to test whether pupillary profiles can be identified within the population.

Sixty-seven healthy adults (18–31 years old; 35 females) completed three pupillometric blocks under controlled ambient illumination using a Tobii Pro Fusion eye-tracker (250 Hz): fixation (2–3 min) to quantify spontaneous oscillations (hippus), a pupillary light reflex (PLR) block to characterise pupil integrity and kinematics, and dynamic emotional face videos to elicit socio-affective dilation. We extracted hippus indices (baseline, frequency, amplitude), PLR metrics (baseline, amplitude, latency, constriction velocity, recovery), and face-evoked dilation measures (baseline, amplitude, latency). Cross-parameter associations were tested using Spearman's rank correlations with correction for multiple comparisons. Robustly normalised features were then clustered using k-means, and cluster separability was assessed with one-versus-rest Receiver Operating Characteristic Curve (ROC) analyses to evaluate clustering discrimination using Area Under Curve (AUC).

Tonic measures of pupil activity were strongly coupled across paradigms, with hippus baseline correlating with baseline during face videos. Baseline pupil diameter was also associated with reflex amplitudes, consistent with a peripheral contribution. Clustering revealed three distinct profiles with good discrimination (AUC $>$ 0.80): a high-tonus/fast profile (short PLR latency, high constriction velocity), a hypo-reactive profile (low tonic level with attenuated PLR and face responses), and a slow/hyper-dilated profile (delayed PLR kinetics with large face-evoked dilation).

Overall, pupil dynamics grouped into three profiles, consistent with an interplay between the tonic central state, autonomic kinematics and iris-related mechanical constraints. This classification cautions against single-mechanism interpretations of pupillary measures, supports individual stratification, and motivates multimodal studies to disentangle central arousal from peripheral gain.

1. Introduction

The eye is the sensory organ responsible for vision: it converts incident light from the environment into neural signals that are processed to guide perception, behaviour, and physiological responses. At the centre of the iris, the pupillary aperture plays an important role in the quality of visual processing (Charman, 2017). Its dilation is linked to retinal illuminance and can enhance visual sensitivity under low-light conditions, at the cost of reduced depth of field and increased optical aberrations (Campbell and Green, 1965). The pupil has an optimal diameter between 2 and 4 mm which tends to optimise optical quality, although the optimum diameter depends on luminance, age, and individual optics (Manion and Stokkermans, 2025). Pupil diameter is controlled by two iris smooth muscles: the sphincter pupillae and the dilator pupillae. These muscles modulate dilation and constriction under autonomic nervous system (ANS) control through sympathetic and parasympathetic pathways. In turn, autonomic output is shaped by widespread brain systems involved in arousal, attention, and cognitive control. In particular, activity in the locus coeruleus–noradrenergic (LC-NE) system covaries with pupil fluctuations, and visuomotor structures

* Corresponding author.
E-mail address: claire.wardak@univ-tours.fr (C. Wardak).

https://doi.org/10.1016/j.ijpsycho.2026.113422
Received 17 February 2026; Received in revised form 18 May 2026; Accepted 19 May 2026
Available online 20 May 2026

such as the superior colliculus (SC) can influence pupil control in contexts involving attention and orienting. Among these mechanisms, the pupillary light reflex (PLR) is a consensual reflex that adjusts retinal illumination in response to changes in light. Although pupillometry has been used to index each of these systems, few studies have assessed their joint contribution across complementary contexts. Here, we integrate hippus, PLR, and face processing within individuals using a unified multivariate framework to identify pupillary profiles and clarify how shared and context-specific mechanisms shape pupil signals.

1.1. From resting pupil to reactivity

Pupil functioning relies on multiple anatomical, biomechanical, and neural factors (Campbell and Green, 1965). A well-controlled way to probe part of these mechanisms is PLR, which provides a readout of photomotor pathway function and the pupil's effector response. The PLR relies on a well-characterised multisynaptic circuit: photoreceptive input arises from rods and cones as well as intrinsically photosensitive retinal ganglion cells (ipRGCs), and signals travel via the optic pathway to the pretectal olivary nucleus, which projects to the Edinger-Westphal nucleus. Preganglionic parasympathetic fibres then travel with the oculomotor nerve to the ciliary ganglion, and postganglionic fibres in the short ciliary nerves innervate the iris sphincter, producing miosis (Joyce et al., 2015; Kelbsch et al., 2019). Importantly, PLR dynamics are not purely 'bottom-up': attention, cognitive load, and emotional salience can modulate reflex gain, consistent with top-down influences from cortical and subcortical systems interacting with autonomic control (Binda and Gamlin, 2017). Beyond the PLR, pupil diameter also exhibits ongoing dynamics that reflect internal state and interactions with environmental stimuli (Pan et al., 2022). At rest, pupil size fluctuates in an oscillatory pattern known as hippus, observed in both adults and children. Yoss and colleagues define the hippus as follows: "A spontaneous and variable bilateral synchronous rhythmic constriction and dilation of the pupils, of sufficient amplitude to be readily visible to the clinician." This pupillary variation arises from the interplay between sympathetic and parasympathetic activation (Bufo et al., 2022). Even under constant luminance, pupil diameter varies with stimulus processing and ongoing neural activity. These changes have been linked with internal processes such as wakefulness (Yamazaki et al., 2023), attentional orientation (Hu et al., 2019), contrast, colour (Gamlin et al., 1998) and motion (Barbur et al., 1992). Additionally, the pupil enables the examination of distinct attention networks (Strauch and Naber, 2022) and social cognition, and is thought to reflect both conscious (Kang and Wheatley, 2015) and preconscious (Laeng et al., 2012) cognitive processes. Crucially, pupil dynamics are influenced not only by subcortical reflexive pathways but also by cortical regions, both visual and non-visual. In particular, activity in the LC-NE system has been shown to correlate with spontaneous pupil fluctuations during states of silent arousal (Reimer et al., 2016) and visual fixation (Yellin et al., 2015), highlighting its role in mediating internal states. However, the relationship between the pupillary response and the variation in physiological arousal remains insufficiently characterised.

Through our work, we aim to clarify the link between the pupil dynamics in different contexts by examining the contributions of three regulatory systems: central state-related influences (LC-NE), autonomic control of pupil kinematics, and biomechanical constraints of the iris.

1.2. System 1: the Locus Coeruleus–Norepinephrine (LC-NE) system

The first system involved in pupil regulation is the LC-NE, which is implicated in vigilance, arousal, and cognitive control. Located in the pons, the LC projects widely throughout the brain and is the principal source of norepinephrine (NE) for the cerebral cortex, cerebellum, and hippocampus (Breton-Provencher et al., 2021). The LC-NE system is often described in terms of phasic bursts superimposed on a tonic baseline. Phasic responses are typically associated with focused attention and task engagement, whereas tonic levels have been linked to distractibility and reduced behavioural specificity (Aston-Jones and Cohen, 2005; Kane et al., 2017). LC tonic activation has been proposed to follow the Yerkes-Dodson law (Aston-Jones and Cohen, 2005), whereby performance varies as a function of arousal level. The LC-NE plays an essential role in the sleep-wake cycle and in state regulation (Berridge et al., 2012; Van Egroo et al., 2022). It is implicated in the compromise between engagement and disengagement and in supporting attention (Sara, 2009) and orientation (Sara and Bouret, 2012), as well as pupillary diameter. The activity of the LC-NE system has been demonstrated to covary with pupillary variations both at rest and during tasks (Reimer et al., 2016; Joshi and Gold, 2020; Joshi et al., 2016; Breton-Provencher and Sur, 2019; Zerbi et al., 2019; Dahl et al., 2022). Indeed, pupil responses following LC activation typically occur on a slow time scale (Larsen and Waters, 2018), and this coupling is modulated by brain state (Yang et al., 2021; Megemont et al., 2024). The LC influence pupil diameter through interactions with the ANS. It modulates the sympathetic branch both directly, through projections to the ciliospinal centre of Budge and Waller, and indirectly via the hypothalamus. Additionally, the parasympathetic branch exerts a direct influence on the Edinger-Westphal nucleus (Szabadi, 2012) and indirectly regulates the SC.

1.3. System 2: the Autonomic Nervous System (ANS)

The second system involved in pupillary control is the ANS, which regulates involuntary physiological functions such as cardiovascular activity, respiration, and ocular responses. It integrates central commands with peripheral feedback which help maintain homeostasis and ensure appropriate responses to internal needs and external demands (Benarroch, 1993). The ANS is composed of two branches in dynamic equilibrium, allowing flexible and rapid physiological adjustments (McCorry, 2007). Sympathetic activity promotes arousal and mobilisation, preparing the body to face challenges by increasing heart rate, respiratory rate, and pupil dilation (Szabadi, 2018; Bradley et al., 2008). Parasympathetic activity supports restorative functions and relaxation, and mediates pupil constriction (McDougal and Gamlin, 2015). Among pupillary responses, the PLR provides the most direct and well-controlled readout of ANS-dependent photomotor function, particularly parasympathetic-driven constriction, making kinematic parameters especially informative under strong stimulus constraints (Kelbsch et al., 2019; Szabadi, 2018). Importantly, autonomic regulation in humans is shaped by top-down cortical influence, particularly from the prefrontal and insular cortices, which are involved in the regulation of visceromotor responses (Benarroch, 1993; Critchley, 2005; Thayer and Lane, 2000). This organisation may support greater flexibility in integrating cognitive and affective signals into autonomic output (Thayer et al., 2009). While the LC-NE system initiates arousal-related neuromodulation and the ANS mediates these signals via peripheral autonomic pathways, it is the iris musculature that ultimately executes pupillary adjustments. This final effector system, composed of smooth muscles under dual autonomic control, plays a crucial role in transforming neural activity into measurable changes in pupil diameter. Understanding its functioning is therefore essential to fully capture how internal states manifest through pupil dynamics.

1.4. System 3: iris musculature

The third system involved in the modulation of pupil dynamics is the iris, a coloured, contractile tissue that forms the pupil aperture and sets the biomechanical limits of constriction and dilation. The iris is part of the uveal tract and lies anterior to the lens, separating the anterior and posterior chambers. It functions as a diaphragm that regulates retinal illumination and influences optical quality (Manion and Stokkermans, 2025). This ocular structure enables the ciliary muscles to accommodate, and influences the focusing of the eye. It also allows the pupil to

change its aperture, resulting in miosis or mydriasis. The iris is a layered, elastic tissue whose stroma contains connective elements, vasculature, and pigment, alongside the contractile smooth muscles. The sphincter is a muscle with a predominant action, comprising circular fibres located in the stroma. The dilator is an external muscle comprising radial fibres and flattened muscle cells located in the bistratified epithelium (Ducasse, 2004). These muscles are under dual autonomic control: parasympathetic activity drives sphincter activation (constriction), whereas sympathetic activity drives dilator activation (dilation). The sympathetic branch innervates the dilator muscle, which can be associated with reduced blood flow to the iris (McDougal and Gamlin, 2015), while parasympathetic activation drives constriction via the sphincter; in parallel, it also controls accommodation via the ciliary muscle. Additionally, the iris is innervated by the ciliary nerves, which contributes to sensory perception within the eye. Importantly, iris biomechanics and optical properties vary across individuals and change with age, contributing to inter-individual differences in baseline diameter, dynamic range, and response amplitude (Strauch and Naber, 2022; Li et al., 2021). By acting as the final interface between autonomic command and pupil response, the iris plays a central role in modulating the amount of light and visual information entering the eye, thereby supporting adaptive physiological and behavioural responses to environmental and internal states.

1.5. Objectives

According to Adaptive Gain Theory, which follows a Yerkes-Dodson function, the LC-NE system contributes to behavioural performance by shaping arousal, responsiveness, and the balance between task engagement and exploration. Tonic pupil diameter is often used as a non-invasive proxy for global arousal and has been shown to covary with LC-NE activity across contexts; however, it is a measure influenced by luminance, autonomic balance, and peripheral constraints. Consequently, tonic pupil diameter may relate to the magnitude and timing of stimulus-evoked pupil responses, although this relationship may vary with context and with peripheral limits (Aston-Jones and Cohen, 2005).

Overall, we hypothesise that pupil dynamics reflect the interaction between central arousal state, autonomic response dynamics, and peripheral biomechanical constraints, such that common pupillary metrics may covary across contexts without mapping onto a single mechanism. Within this framework, it is difficult to associate a given pupillary measure with a single mechanism, because the different systems involved in pupil control interact with one another. Nevertheless, tonic baseline measures were considered to primarily index central state-related influences, including LC-NE-related arousal; PLR temporal and velocity parameters were considered to preferentially reflect autonomic response dynamics, particularly parasympathetically driven constriction; and amplitude-related measures were expected to be shaped by peripheral iris contractile and biomechanical constraints. In line with this framework, we predict that an optimal arousal level within the LC-NE system, indexed by tonic pupil diameter, will be associated with an adaptive phasic pupil response across contexts. We also predict that inter-individual differences in ANS reactivity will be expressed primarily in the speed of pupillary responses, such that kinematic parameters capture autonomic responsiveness under strong stimulus constraints. Finally, we expect peripheral smooth-muscle and biomechanical capacity of the iris to impose limits on constriction and dilation, thereby shaping amplitude-related measures across paradigms.

To investigate these interdependencies, we used three complementary pupillometric paradigms designed to dissociate reflexive, resting-state, and socio-affective components of pupil control: a PLR paradigm to characterise parasympathetically-driven constriction kinematics and amplitude limits; a fixation-rest paradigm to capture spontaneous pupil dynamics (hippus) under low task demands; a social perception paradigm using human faces, a highly salient stimulus category for adults, who show specialised and efficient face processing (Carey, 1992). Faces often elicit pupil dilation, consistent with increased cognitive and affective processing demands (Aguillon-Hernandez et al., 2020; Ricou et al., 2024). Together, these paradigms allow us to examine how baseline pupil diameter, reflex kinematics, and stimulus-evoked responses covary or dissociate across contexts, thereby informing the relative contributions of central state, autonomic dynamics, and peripheral constraints to pupil signals.

2. Method

2.1. Participants

Sixty-seven participants (35 females) aged between 18 and 31 years ($M = 23.21 \pm 3.30$) were recruited for the study. This age range was selected to minimise interindividual variability in pupil diameter. Exclusion criteria included uncorrected vision, a history of psychiatric, neurological, or neurodevelopmental disorders, as well as learning disabilities or difficulties with walking or speech development. All participants provided written informed consent prior to participation. The study received approval from ethical committees (CPP, PROSCEA 2017-A00756-47, SIRCUS 2022-A00870-43) and was conducted in accordance with the ethical principles outlined in the Declaration of Helsinki for research involving human subjects (World Medical Association, 2013).

Based on our statistical strategy (see 2.5), we aimed to recruit between 60 and 70 participants. First, we planned to run correlation analyses. To have enough power to observe a medium correlation with $\rho = 0.4$, alpha $= 0.05$ and power $= 0.95$, a sample size of 63 is required (G*Power®). Second, we planned to run k-means cluster analyses. Based on previous work (Rabadan et al., 2026), we expected at least two clusters based on median pupil size. Previous pupillary studies using clustering and obtaining 2 clusters varied from 30 participants (e.g. Rabadan et al., 2026) to 70 participants (e.g. Alshanskaia et al., 2024), but the number of participants required depends mainly on the separability of the clusters (Dalmaijer et al., 2022).

2.2. Stimuli and protocol

The protocol consisted of three stimulus blocks, designed to probe complementary components of pupil control: fixation (hippus), pupil light reflex, and emotionally expressive face videos (Fig. 1). These blocks were selected from a broader research protocol and were presented within a single session.

2.2.1. Hippus (fixation)

Participants fixated a black cross ($X = 960$ px, $Y = 765$ px; apparent width: 1.80°, height: 1.96°, thickness: 0.16°) on a uniform grey background for 2–3 min. They were instructed to remain still and maintain fixation. The screen illuminance at the participant's eye level during this block was 5.5 lx.

2.2.2. Pupillary light reflex (PLR)

Five alternating black and white full-screen were presented, each lasting 5 s, for a total of 50 s. Participants were only asked to look at the screen and remain silent throughout the duration of the recording. This block was designed to assess pupil reactivity to luminance changes and evaluate reflex integrity. Screen illuminance alternated between 0.5 lx during black screens and 12 lx during white screens (measured at eye level).

2.2.3. Face videos

Eight 4-s videos of human faces displaying emotional expressions were presented in random order. The stimuli were drawn from a prior validated paradigm (Ricou et al., 2024) focused on social and motion perception. The videos featured four actors (two females), each expressing happiness or sadness. A visual example of the face-video

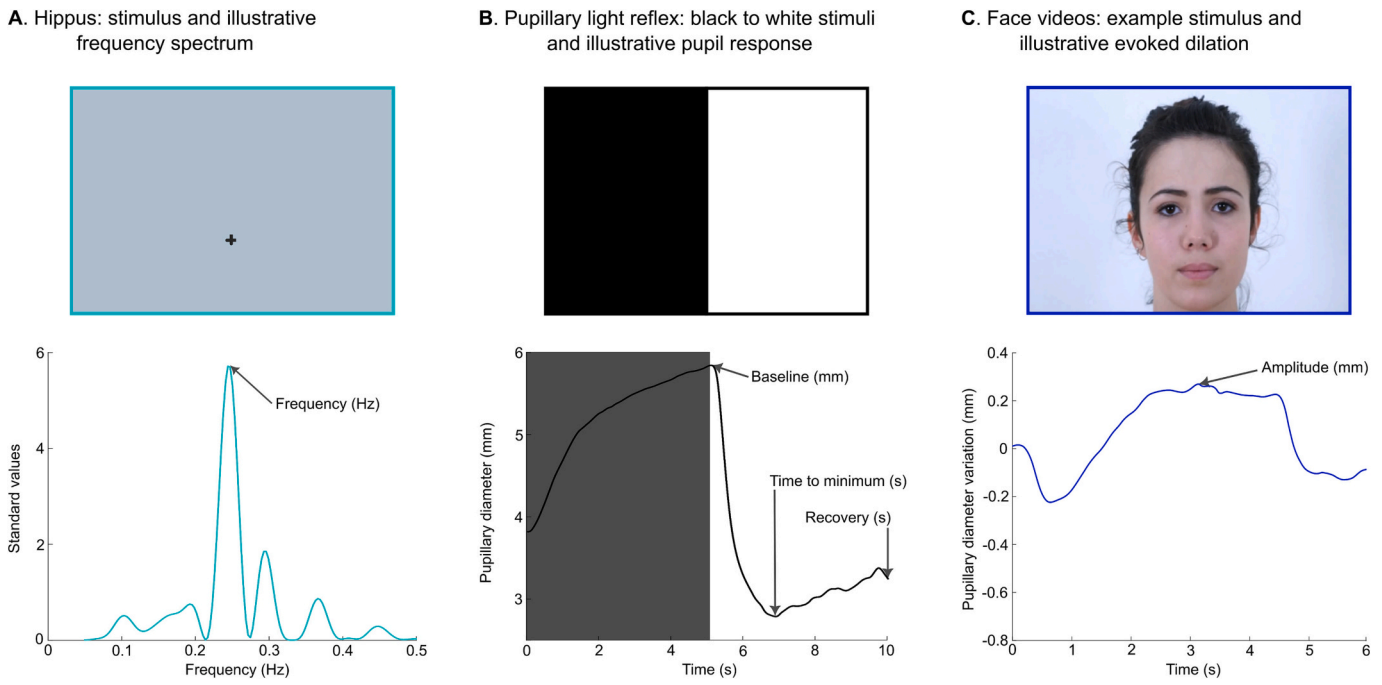

Fig. 1. Experimental paradigms and representative signals for hippus, PLR, and face videos. (A) Hippus: stimulus and illustrative frequency spectrum. Schematic of the hippus block and representative frequency spectrum highlighting the dominant oscillatory components of spontaneous pupil activity. (B) Pupillary light reflex: black to white stimuli and illustrative pupil response. Schematic of the luminance step (black-to-white) and a pupil time course showing the characteristic light-evoked constriction followed by re-dilation. (C) Face videos: example stimulus and illustrative evoked dilation. Example frame from the face-video stimulus and a pupil-dilation time course illustrating the evoked response during face viewing. Coloured contours indicate block type (as used in Figs. 2–5) and were not presented. The colour code was as follows: Hippus (cyan), PLR (black), and face videos (navy blue). (For interpretation of the references to colour in this figure legend, the reader is referred to the web version of this article.)

stimuli is provided in Ricou et al. (2026) (Ricou et al., 2026). All stimuli were standardised for duration and colorimetry. For all face-video stimuli, the background colour was identical across actors, with an RGB value of 210, 220, 238. To further quantify the visual properties of the stimuli, contrast ratios between the background and the foreground face region were calculated from relative luminance using the following formula: (Luminosity light +0.05) / (Luminosity dark + 0.05). The foreground was estimated from the skin colour of each actor. The RGB values and contrast ratios were as follows: first female actor, RGB = 192, 162, 161, contrast ratio = 1.65:1; second female actor, RGB = 186, 164, 169, contrast ratio = 1.68:1; first male actor, RGB = 219, 183, 196, contrast ratio = 1.26:1; and second male actor, RGB = 195, 166, 172, contrast ratio = 1.64:1.

In-between each video, an inter-trial image composed of a uniform grey background and a central black cross (located at the level of the mouth) was presented for 2 to 4 s. Participants were only asked to look at the screen and remain silent throughout the duration of the recording. Across the face-video and inter-trial periods, mean screen illuminance at eye level was kept constant at 5.5 lx.

2.3. Materials

Eye-tracking data were recorded using a Tobii® Pro Fusion eye-tracker which was placed 1 cm below the screen. This tool has a sampling frequency of 250 Hz, an accuracy of 0.3°, and a precision of 0.04°. Our protocol was run with Tobii® Pro Lab. Each participant was seated in a chair in front of the monitor, approximately 70 cm away. All recordings were conducted in the same experimental tent to control luminosity and allow repeatability of measurement with an ambient light level of 4 lx. Before starting the eye-tracking recordings, a calibration procedure was performed followed by a four-points validation. Calibration was deemed successful if the precision during the validation was below 1.00°. Otherwise, the calibration procedure was repeated until such a precision was reached. The protocol was displayed in the centre of a 27″ monitor with a resolution of 1920 × 1080 pixels and a refresh rate of 60 Hz. The tent was illuminated by an adaptable LED light positioned behind the screen.

2.4. Data processing

2.4.1. General preprocessing

Raw pupil data were exported from Tobii pro-lab and processed using custom scripts in MATLAB® and RStudio®.

For the hippus and face video blocks, we plotted the pupil diameter for each participant to verify the integrity of the data. When data gaps were identified, we performed 1-D interpolation to fill these gaps using the 'nearest' (Nearest neighbor interpolation: the interpolated value at a query point is the value at the nearest sample grid point) method. To remove blinks from our recordings, we computed the first derivative of pupil diameter (blink speed). Using this signal, we detected the onset and offset of each blink.This allowed us to eliminate blinks for each eye. Subsequently, a second correction was applied by comparing the pupil vectors of each eye. Blinks were replaced with interpolated values from the 70 preceding and succeeding diameter values. Once these steps were completed, we applied a median filter [120] and a Butterworth filter (1,20/500/2). These two filters were used to smooth the interpolated data and remove high-frequency noise. For the pupil light reflex block, the same steps were performed, but directly on the average pupil diameter of both eyes. After this preprocessing, we segmented the recordings by stimulus for the pupil light reflex and videos of faces blocks.

2.4.2. Hippus parameters extraction

For the hippus, the overall processing steps followed the description in previous work (Rabadan et al., 2026), adapted for the differences in eye-tracking acquisition parameters. We averaged the diameter of both eyes, and the recordings were trimmed by deleting points at the

beginning and end of each block. We then selected the best part of each recording (≥ 11,250 samples). Three parameters were calculated: the baseline pupil diameter, the frequencies of pupil variation and the amplitude of these frequencies. The baseline diameter corresponding to the median was calculated per participant. To assess pupil variations and their stability during each block, we performed a series of steps using a 30 s sliding time window (1 s steps, i.e. 96.66% overlapping). First, to obtain a spectrum of the signal, we applied a) a 1 × 3 one-dimensional median filter to smooth the signal and remove impulse noises, b) a second order Butterworth bandpass filter with a cut-off frequency [0.15 1.0] Hz to remove the harmonic frequencies, and c) a Fast Fourier Transform for spectral analysis. To carry out the spectral analysis over our 30 s sliding window while maintaining good resolution, we interpolated our 30 s signals using an 81920-point nfft (nonuniform Fast Fourier Transform). Accuracy was therefore increased from 0.033 Hz to 0.000101725 Hz (Δf = (SF/(N*T); f: frequency in Hz, N: number of points = 81,920, SF: sampling frequency = 250 Hz, T: time in s = 30 s). Once the frequency spectra were obtained, the maxima on each spectrum were labelled and extracted. Then, we calculated the median frequency over all the sliding windows. When measuring amplitude and baseline pupil diameter, we used the same sliding window of 30 s. We measured the amplitude by adding up the absolute values of the extrema of a window. Following these processing steps, we calculated the median amplitude and baseline over all the sliding windows.

This processing resulted in three hippus parameters extraction: hippus baseline, hippus frequency, and hippus amplitude.

2.4.3. PLR parameters extraction

For the processing of pupil light reflex, only one PLR response was retained for each participant because signal quality varied across repetitions in this block. The selected response corresponded to the trial with the highest signal quality, defined as the reflex containing the lowest proportion of interpolated data while allowing reliable extraction of all parameters. This choice was made to minimise artefact-related noise in the estimation of PLR parameters. However, because this could lead to the selection of different trial across participants, we performed an analysis to assess whether the selected PLR trial was associated with the extracted PLR parameters. The selected signal was then processed to extract the parameters of interest. Processing included median filtering [1 5] to suppress impulsive noise, followed by zero-phase low-pass filtering (1, 0.1) to attenuate high-frequency components. The signal was subsequently fitted with a fifth-order polynomial, and a final median filter [1 10] was applied to reduce residual artefacts and ensure signal smoothness. Once these steps are completed, we extracted the parameters using the slope method. This method consisted of detecting a tilt of 0.08 s (20point) to extract the maximum and minimum parameters of the reflex. The maximum pupil diameter immediately preceding constriction was used as the PLR baseline parameter. This is consistent with previous pupillometry studies in which baseline pupil diameter is included as a core PLR parameter and used as a physiological reference (Cortez et al., 2017). The pupillary diameter was also extracted at the end of the reflex (end of the white flash), corresponding to our measurement of the recovery of the pupillary light reflex.

This processing resulted in the following parameters extraction: PLR baseline, PLR constriction amplitude, PLR time to minimum, PLR constriction velocity, and PLR recovery.

2.4.4. Face video parameters extraction

For the videos of faces, we verified the integrity of our 8 trials individually. Once the recordings were verified, we averaged the trials together. This allowed us to extract on pupil dilation the maximum, latency, and median parameters. We measured the maximum between 1100 ms and 4800 ms (this interval was chosen to account for the entire pupillary dynamics), and the latency of this maximum. Baseline pupil diameter was computed for each trial as the median pupil diameter across the 260 data points preceding video onset, corresponding to the stable pre-stimulus period. These trial-level baseline values were then averaged within each participant to obtain a single face-video baseline parameter.

This processing resulted in the following parameters extraction: face videos baseline, face videos amplitude (maximum), and face videos latency.

2.5. Statistical analyses

Statistical analyses were performed using RStudio® (v4.1.1). Three categories of pupillary metrics were analysed: hippus (baseline, frequency, and amplitude), pupil light reflex (baseline, time to minimum, constriction amplitude, constriction velocity, and recovery), and face evoked pupil responses (baseline, amplitude, and latency). Descriptive statistics are reported for all variables as median and interquartile range (median [IQR]) and as mean and standard error (mean [SE]). Prior to analyses, distributional assumptions were inspected using q-q plots generated with the qqnorm() and qqline() functions from the stats package (Bolar, 2019), and homogeneity of variances was assessed using Levene's test with the leveneTest() function from the car package (Fox et al., 2026).

2.5.1. Correlational analyses

Associations between pupillary parameters were assessed using Spearman's rank correlations with the stats package (Bolar, 2019) (cor.test()). To limit error due to multiple testing, *p*-values were corrected using the Bonferroni method with the p.adjust() function from the stats package (Bolar, 2019). Only statistically significant associations (Bonferroni-corrected $p < 0.05$) are reported. In addition to linear monotonic associations, potential quadratic relations between variable pairs were explored. We calculated the correlation matrix using the cor() function from the stats package (Bolar, 2019) and employed the corrplot package (Wei et al., 2024) to visualise this matrix graphically. To quantify cross-context changes while accounting for interindividual differences in baseline, we computed a relative change index for each pupillary parameter at the participant level. Specifically, for each amplitude parameters and context, values were expressed as a relative change from the corresponding baseline reference. We then assessed Spearman correlations between baseline measures and delta across participants and context. *P*-values were corrected for multiple comparisons using the same Bonferroni procedure as described above.

2.5.2. Clustering and ROC analysis

All parameters were extracted and organised in a file. We then normalised variables by family: baseline diameters (hippus baseline, PLR baseline, and face videos baseline) were normalised together, and PLR constriction amplitude and PLR recovery were normalised together. Robust normalisation was performed using the median and interquartile range (IQR), ((median value – median of the data set) /Interquartile Range) computed with the median() and IQR() functions from the stats package (Bolar, 2019). We performed clustering on our normalised data using the k-means method via the stats package (Bolar, 2019) (kmeans()). To determined how many clusters we could identify, we computed silhouette scores using the silhouette() function from the cluster package (Maechler et al., 2026) and an elbow plot, which converged toward the identification of 3 clusters. Once our clusters were identified, we performed one-versus-rest ROC analysis on the parameters of each cluster to understand which parameters allowed us to separate our populations. ROC analyses were performed using an in-house MATLAB® script, and the area under the curve (AUC) was computed for each parameter. For this analysis, we considered a good discrimination performance when the obtained AUC value is ≥0.80.

2.5.3. Associations with individual factors

Associations between cluster membership and categorical

participant characteristics (sex, eye colour, ocular dominance, manual dominance and daytime recording period) were tested using Pearson's chi-square tests with the chisq.test() function from the stats package (Bolar, 2019) when expected cell counts were sufficient, and Fisher's exact tests were additionally reported as a robustness check using the fisher.test() function, particularly for unbalanced group sizes. When an overall association was significant, post hoc inspection relied on standardised residuals and pairwise Fisher's exact tests with Bonferroni correction using p.adjust() from the stats package (Bolar, 2019). Age differences between clusters were evaluated using the Kruskal–Wallis test with the kruskal.test() function.

2.5.4. Regression analyses

Multiple linear regression models were conducted with stats package (Bolar, 2019) using the lm() function to assess the contribution of individual factors (sex, age, eye colour, ocular dominance, manual dominance) to pupillary parameters with correction for multiple comparisons (Bonferroni method).

2.5.5. Pupil light reflex quality verification

To assess whether the selected PLR trial was associated with the extracted PLR parameters, the trial was treated as a categorical variable. Given the strong imbalance in the distribution of selected trial, non-parametric tests were used. First, Kruskal–Wallis tests were performed with the kruskal.test() function from the stats package (Bolar, 2019) to compare PLR parameters across selected trial from 1 to 5. Second, because most selected PLR responses corresponded to the first trial, participants were grouped according to whether trial 1 or trials 2–5 had been selected. Wilcoxon rank-sum tests were then performed with the wilcox.test() function from the stats package (Bolar, 2019) to compare PLR parameters between these two groups. The tested PLR parameters were PLR baseline, time to minimum, constriction amplitude, constriction velocity, and recovery. *P*-values were corrected for multiple comparisons using the Bonferroni method with the p.adjust() function from the stats package (Bolar, 2019). To further assess whether the PLR trial-selection procedure influenced the clustering analysis, we also tested the association between the selected PLR trial and cluster membership. Fisher's exact tests were performed with the fisher.test() function from the stats package (Bolar, 2019), first by considering selected trial number as a five-level categorical variable and then by grouping participants according to whether trial 1, or trials 2–5 had been selected. *P*-values were corrected for multiple comparisons using the Bonferroni method.

2.6. Visualization

For the creation of the figures intended for the article, we used R software and the ggplot2 package (Wickham et al., 2026). Specifically, we used the ggradar() function from the ggplot2 package (Wickham et al., 2026) to create radar plots, the mosaicplot() function from the graphics package (Murrell, 2020) to create mosaic plots, and the ggcorrplot() function from the ggplot2 package (Wickham et al., 2026) to visualise the correlation matrix. These plots allowed for a clear visual representation of the analysis results. To finalise the formatting of the figures, we used Inkscape software (v.0.92.3), which enabled us to adjust graphical elements and enhance the presentation.

3. Results

Sixty-seven adults were included; one participant, an outlier across all measures, was excluded a priori, yielding a final sample of $N = 66$. We aimed to examine resting oscillations (hippus), PLR dynamics, and face-evoked response parameters to test our hypotheses.

3.1. Descriptive characteristics of the data

Fig. 2 presents the group-mean pupil signal for the Pupil light reflex (PLR) and Face videos blocks, and an illustrative single-participant trace for the Hippus block. As expected, we observed pupillary oscillations (hippus) in the Hippus block, a dilation followed by a constriction and a re-dilation in the PLR block, and finally a dilation following face presentation in the Face videos block. We report in Table 1, for each variable, the median, the interquartile range [IQR], the mean and standard error [SE].

Overall, central tendency and dispersion were modest for most variables; hippus frequency showed the tightest spread, whereas PLR baselines and amplitudes displayed broader variability.

3.2. Hypothesis-aligned correlational analyses

3.2.1. LC-NE system hypothesis: optimal arousal and adapted pupillary responses

We tested whether tonic indices (hippus baseline and face videos baseline) predict the magnitude of the phasic response (face videos amplitude).

No association was observed between face videos amplitude and either the hippus baseline or face videos baseline. By contrast, hippus baseline correlated strongly with face videos baseline ($\rho = 0.81$, $p = 5.86 \times 10^{-14}$), indicating that a common underlying tonic state modulates both spontaneous oscillations and baseline level (Fig. 3). Within the LC-NE framework, these results indicate tonic coupling without a phasic counterpart in this paradigm.

3.2.2. Autonomic nervous system (ANS) hypothesis: reactivity and pupillary kinematics

We next evaluated whether hippus frequency correlates with dynamic parameters of the PLR and with the face videos latency of face-evoked dilation.

No correlations were found between hippus frequency and PLR time to minimum, PLR constriction velocity, or face videos latency. Likewise, face video latency did not correlate with either PLR time to minimum or PLR constriction velocity. In this context, hippus frequency provides no evidence for a link with the ANS-dependent kinematic examined.

3.2.3. Iris hypothesis: contractile properties and response amplitudes

We tested the hypothesis that contractile properties of the iris are reflected in spontaneous oscillations (hippus), PLR parameters, and face-evoked dilation.

Several associations support a determining role of iris smooth-muscle properties in diameter variations. The PLR baseline correlated with hippus baseline ($\rho = 0.65$, $p = 2.25 \times 10^{-7}$) and with PLR constriction amplitude ($\rho = 0.76$, $p = 5.36 \times 10^{-12}$). Moreover, hippus baseline correlated with hippus amplitude ($\rho = 0.42$, $p = 2.23 \times 10^{-2}$) as well as with PLR constriction amplitude ($\rho = 0.45$, $p = 8.44 \times 10^{-3}$). A positive correlation between PLR time to minimum and PLR constriction amplitude was also observed ($\rho = 0.55$, $p = 2.02 \times 10^{-6}$). By contrast, face videos amplitude correlated with neither PLR time to minimum nor PLR recovery. Taken together, these findings support the view that inter-individual differences in iris tonus and biomechanics are coherently expressed in baseline levels, spontaneous oscillations, and reflex responses (Fig. 3). We also tested for quadratic relations across all examined variable pairs, no significant effects were detected.

3.3. Additional correlations

As a complement, we examined other correlations. Face videos baseline, which may capture central tonic components in addition to peripheral constraints, was associated with hippus amplitude ($\rho = 0.54$, $p = 1.81 \times 10^{-4}$) and with PLR constriction velocity ($\rho = 0.45$, $p = 8.44 \times 10^{-3}$). These links are less specific as they may reflect mixed (central

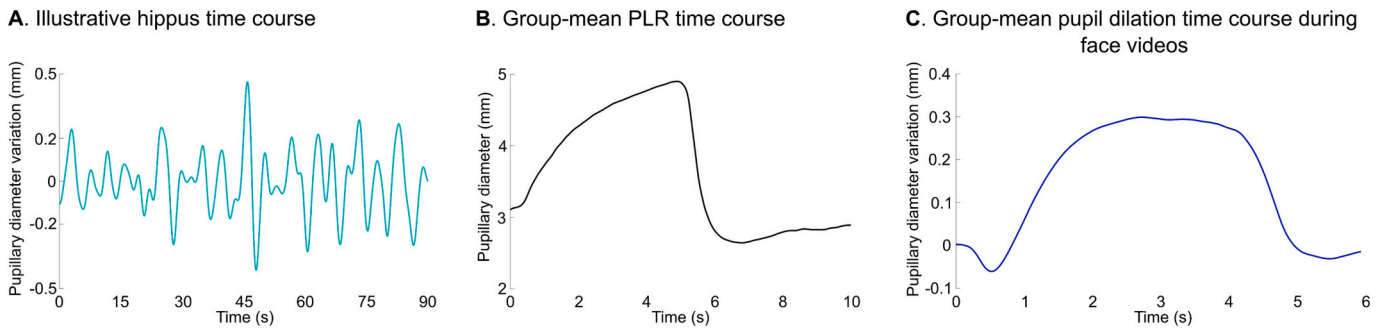

Fig. 2. Pupil time courses across paradigms. (A) Illustrative hippus time course, showing pupil diameter fluctuations from a single participant during the hippus block. (B) Group-mean PLR time course, showing the pupillary light reflex averaged across participants. (C) Group-mean pupil dilation time course during face videos, showing face-evoked pupil dilation averaged across participants.

Table 1
Descriptive statistics of pupillary parameters across paradigms. Summary statistics are reported for each pupillometric measure extracted from the Hippus, pupillary light reflex (PLR), and Face videos blocks. For each parameter, values are provided as median and interquartile range (Median [IQR]) and as mean and standard error (Mean [SE]). Units are as follows: frequency (Hz), pupil diameter and amplitude (mm), time (s), constriction velocity (mm/s), and latency (ms).

	Parameter	Median [IQR]	Mean [SE]
Hippus	Frequency (Hz)	0.186 [0.063]	0.187 [0.005]
	Baseline (mm)	3.317 [0.616]	3.3445 [0.057]
	Amplitude (mm)	0.674 [0.268]	0.695 [0.024]
Pupil light reflex	Baseline (mm)	5.127 [1.073]	5.087 [0.081]
	Time to minimum (s)	1.592 [0.637]	1.613 [0.061]
	Constriction amplitude (mm)	2.507 [0.678]	2.468 [0.058]
	Constriction velocity (mm/s)	1.599 [0.509]	1.628 [0.052]
	Recovery (s)	0.217 [0.302]	0.240 [0.032]
Face videos	Baseline (mm)	3.564 [0.689]	3.610 [0.068]
	Amplitude (mm)	0.362 [0.180]	0.357 [0.019]
	Latency (ms)	3422 [1431]	3389.757 [99.946]

and peripheral) contributions (Fig. 3). Within the PLR itself, constriction velocity was strongly negatively correlated with time to minimum ($\rho = -0.798$, $p = 1.74 \times 10^{-9}$), a relationship expected because both parameters index the same constriction phase and are mathematically and mechanistically coupled; therefore, this association provides limited additional physiological insight beyond confirming internal consistency of PLR kinematics. To account for interindividual differences in baseline and test whether baseline levels relate to response changes across contexts, we performed additional delta correlation analyses; however, no significant associations were observed after Bonferroni correction.

3.4. Clustering of pupillary profiles and ROC validation

After robust normalisation by variable families (baseline diameters grouped; PLR constriction amplitude and recovery grouped), k-means clustering was applied. Validation metrics (silhouette and elbow) converged on a three-cluster solution. To characterise each cluster, ROC analyses were conducted, using an informative performance of AUC $\geq$ 0.80.

This approach revealed three distinct pupillary profiles. The first, corresponded to a "high tonus" profile, discriminated by short PLR time to minimum (AUC = 0.85) and high PLR constriction velocity (AUC = 0.92); face videos baseline diameter was also higher (AUC = 0.80), and this profile combines elevated tonic level with rapid reflex kinematics. The second profile, termed "hypo-reactive," was defined by low hippus baseline (AUC = 0.82), low PLR baseline (AUC = 0.88), and low PLR constriction amplitude (AUC = 0.83); it also shows very low face videos amplitude (AUC = 0.96), suggesting a flattening of both reflex and stimulus dependent responses. The third profile, labelled "slow/hyper-dilated," combined a very long PLR time to minimum (AUC = 0.96) and slow PLR constriction velocity (AUC = 0.86), with very large face videos amplitude (AUC = 0.82). This last profile combines delayed kinematic with large phasic responses.

Together, these three profiles capture distinct pupillary dynamics that differentially articulate tonic level, spontaneous oscillations, and reactivity (Figs. 4 and 5).

3.5. Individual factors and cluster distribution

We tested the association between individual variables and cluster membership. Age did not differ significantly between clusters. In contrast, a significant difference in cluster distribution was observed for sex ($\chi^2(2) = 8.53$, $p = 0.014$; Fisher's exact test $p = 0.016$). Post hoc analyses based on standardised residuals revealed an over-representation of females in Cluster 2 and of males in Cluster 3 (Fig. 6). Pairwise Fisher's exact tests confirmed a significant difference between Cluster 2 and Cluster 3 after Bonferroni correction ($p = 0.031$). A trend toward an effect of eye colour was also observed ($\chi^2(2) = 5.84$, $p = 0.054$; Fisher's exact test $p = 0.055$) (Fig. 6). Although a higher proportion of dark-eyed participants was present in Cluster 2, post hoc pairwise comparisons did not remain significant after correction for multiple testing. No associations were observed between cluster membership and daytime recording period, ocular dominance, or manual dominance. Multiple linear regression analyses were further conducted to evaluate simultaneously the contribution of these variables to the outcome parameters; however, no predictor showed a statistically significant association after correction for multiple testing.

3.6. Pupil light reflex quality

As a control analysis, we examined whether the selected PLR trial was associated with the extracted PLR parameters. Kruskal-Wallis tests comparing selected trial revealed no significant effect of trial on PLR baseline, time to minimum, constriction amplitude, constriction velocity, or recovery after Bonferroni correction. Because most selected responses corresponded to the first PLR trial, we additionally compared participants for whom trial 1 was retained with those for whom trials 2 to 5 were retained. Wilcoxon tests showed no significant differences after Bonferroni correction. Overall, these analyses did not provide evidence that the selected PLR trial systematically influenced the extracted PLR parameters. We further examined whether the selected PLR trial was associated with cluster membership. Fisher's exact tests showed no significant association between cluster membership and the selected PLR trial, either when trial was considered with five levels, corresponding to trials 1 to 5, or when participants were grouped according to whether trial 1 or trials 2–5 had been selected. These results remained

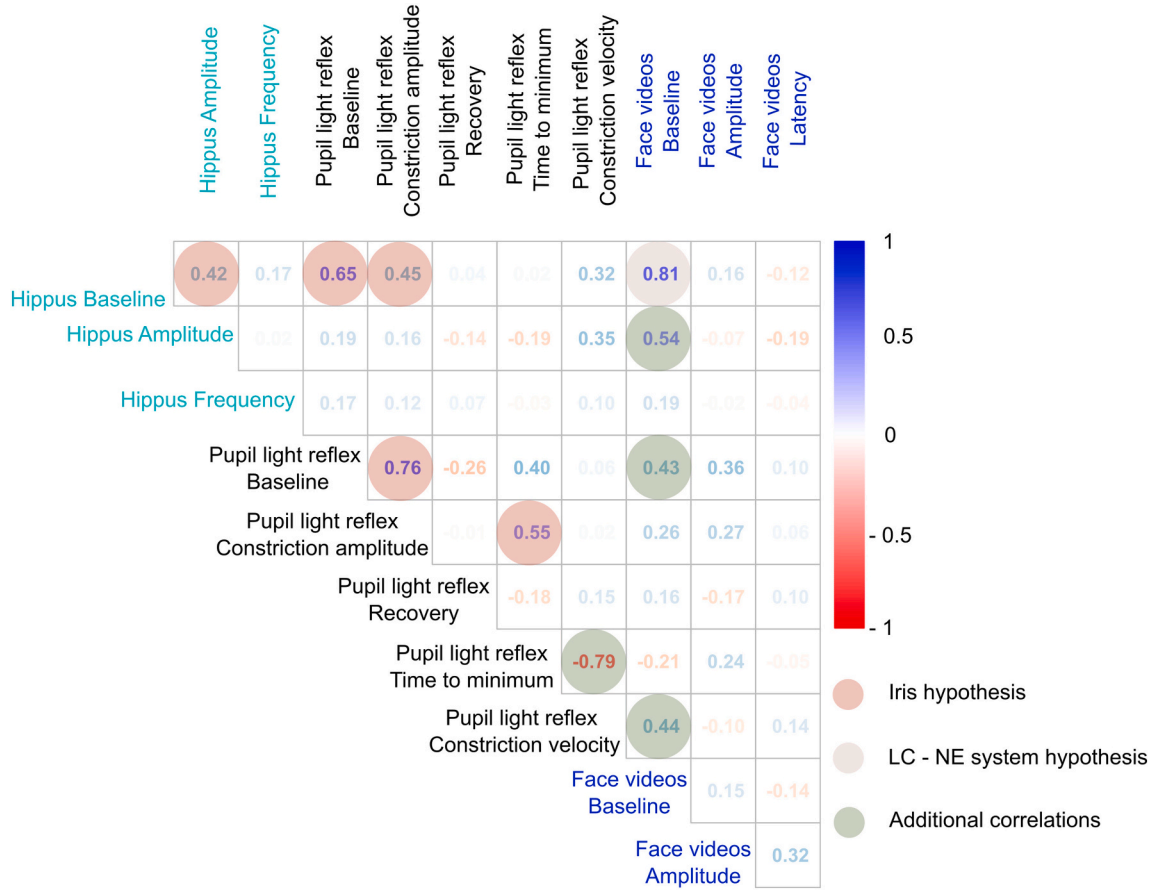

Fig. 3. Hypothesis-driven correlations across LC–NE, ANS, and iris-related pupil measures. Spearman's rank correlation coefficients (ρ) were computed for all pairwise associations and displayed as a correlation matrix. Correlation coefficients are colour-coded on a blue-red gradient (dark blue: strongly positive; dark red: strongly negative), and numerical ρ values are reported in each cell. *P*-values were Bonferroni-corrected; correlations with corrected $p < 0.05$ and $|\rho| > 0.40$ are highlighted. Coloured contours indicate hypothesis category. The colour code was as follows: iris hypothesis (pastel red), LC–NE hypothesis (pastel grey), and additional correlations (pastel green). (For interpretation of the references to colour in this figure legend, the reader is referred to the web version of this article.)

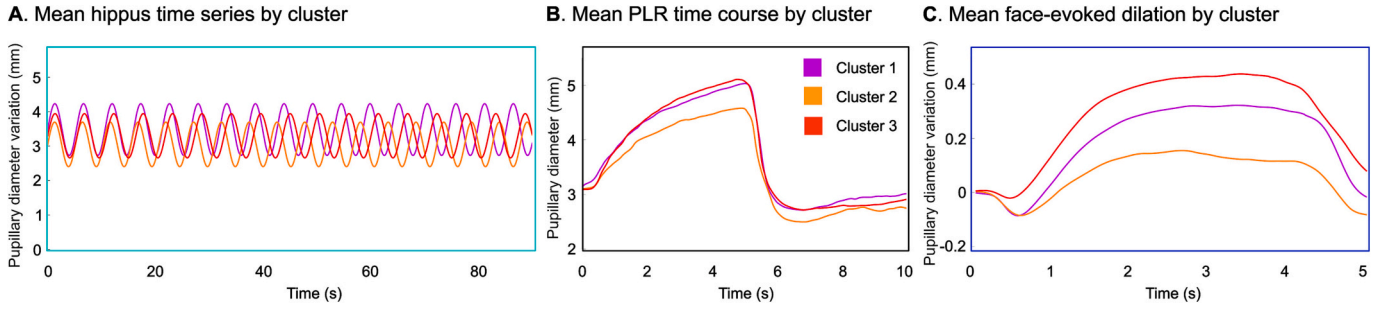

Fig. 4. Average pupil dynamics by cluster reveal distinct signatures. (A) Mean hippus time series by cluster, showing a signal reconstructed a posteriori using hippus parameters estimated from the populations of the three clusters. (B) Mean PLR time course by cluster, showing the pupillary light reflex averaged across individuals within each cluster. (C) Mean face-evoked dilation by cluster, showing pupil-dilation time course during face-video blocks averaged across individuals within each cluster. Cluster identity is colour-coded (as used in Figs. 5 and 6). The colour code was as follows: cluster 1 (purple), cluster 2 (orange), and cluster 3 (red). (For interpretation of the references to colour in this figure legend, the reader is referred to the web version of this article.)

non-significant after Bonferroni correction. Thus, the distribution of participants across clusters did not appear to be driven by the PLR trial-selection. However, because selected trial groups were strongly imbalanced and the analysis could not assess within-subject changes across PLR repetitions, these results should be interpreted with caution.

4. Discussion

In this study, we used eye tracking to characterise the pupil and its dynamics across three complementary contexts: rest, to capture spontaneous oscillations (hippus); the pupillary light reflex (PLR), to quantify pupil dynamics that are primarily parasympathetically driven; and face perception, to assess socio-affective reactivity. The central aim was to disentangle three partially independent axes: a central tonic arousal axis, indexed by baseline-level measures and slow oscillations, which we expected to influence the amplitude of evoked dilation; an autonomic kinematics axis, indexed by timing and velocity parameters; and a peripheral contractile axis, linked to iris biomechanics and expressed

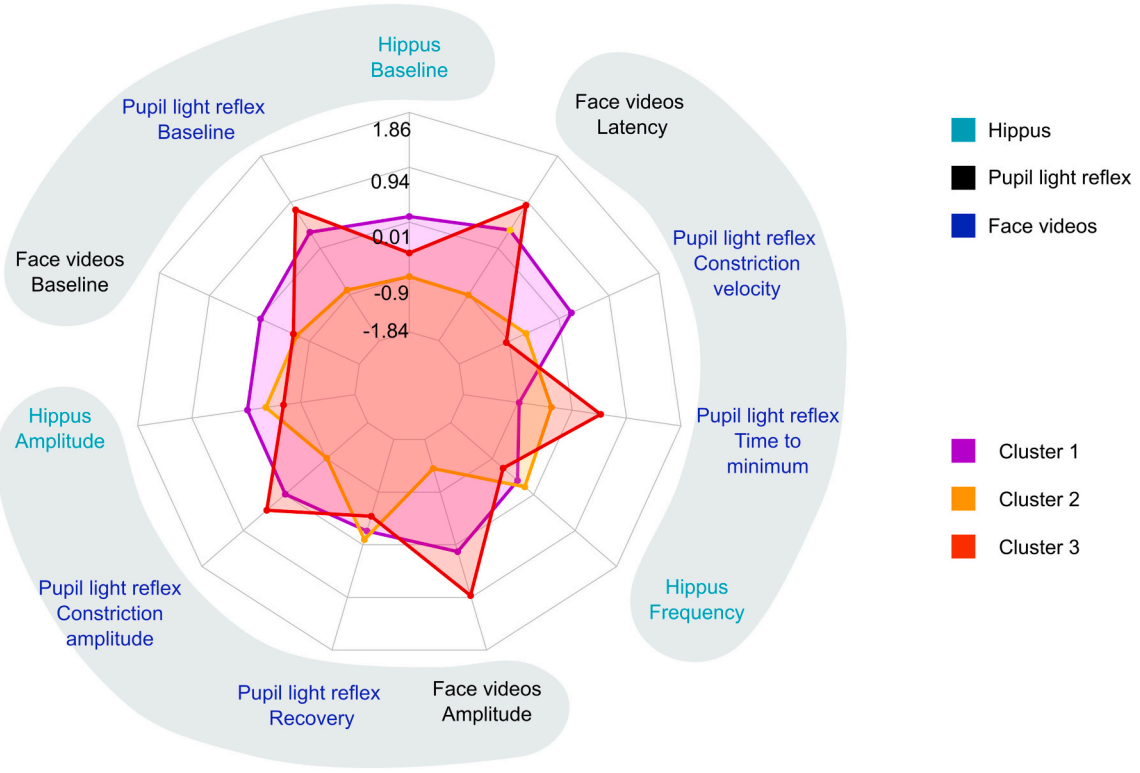

Fig. 5. Multidimensional cluster profiles across pupillary parameters. Radar plots depict cluster profiles across pupillary parameters. Each axis corresponds to one parameter, and the radial magnitude reflects the cluster-level value for that parameter. Parameters are organised into three domains: Baseline, Amplitude, and Kinematics.

Fig. 6. Associations between cluster membership and sex and eye colour. (A) Cluster distribution by sex. (B) Cluster distribution by eye colour. Mosaic plots show the distribution of participants across clusters by sex and by eye-colour category. Colours encode category membership. The colour code was as follows: females and light eye colour (taupe), and males and dark eye colour (dark grey).

mainly in amplitude parameters. These axes interact without merging: the pupil is a multi-determined signal, in which common metrics may emerge across several contexts without mapping onto a single mechanism. The same metrics can reflect distinct physiological levels depending on context and stimulation constraints. We therefore sought to describe the architecture of these pupillary responses by highlighting covariations and dissociations across contexts, using a multivariate approach to identify pupillary profiles combining evoked responses, tonic level, and peripheral constraints.

The results support this dissociation. The baseline of hippus covaries with baseline diameter, including immediately before face exploration, suggesting a shared tonic state over a timescale of a few seconds. This interpretation aligns with work showing that, at rest, spontaneous pupil fluctuations covary with activity in nuclei of the ascending arousal system and with variations in cortical state (Lloyd et al., 2023; Schneider et al., 2016). This link is documented by resting-state pupil-fMRI correlations, as well as by probabilistic fMRI decoding approaches linking the pupil to the fidelity of sensory representations (Lloyd et al., 2023; Geurts et al., 2024; Sobczak et al., 2021). Beyond this, it converges with the view that the pupil reflects a multi-system arousal signal (Joshi and Gold, 2020; Joshi et al., 2016; Murphy et al., 2014). By contrast, these tonic indices do not predict the maximum dilation amplitude to faces: the social phasic response is therefore not a simple reflection of background tone. We also found no evidence for a quadratic (inverted-U) relationship between tonic indices and face-evoked dilation, as sometimes reported for pupil diameter within the adaptive-gain theory (Murphy et al., 2011). It is consistent with the engagement of additional determinants linked to social salience and to the dynamic properties of

faces (social content, facial motion, perceived proximity), which are known to amplify pupillary dilation independently of baseline arousal level (Ricou et al., 2024; Kret et al., 2013; Bogdanova et al., 2022).

Hippus frequency is associated with neither constriction time to minimum nor constriction velocity, indicating that it primarily reflects tonic background arousal rather than the functioning of the fast parasympathetic loop governing the initial phase of the PLR. This dissociation is compatible with the idea that hippus reflects the integration of low- and high-level factors (Rabadan et al., 2026), whereas early PLR kinematics depend strongly on sphincter dynamics under parasympathetic control (Marumo and Nakano, 2021). It is also consistent with the fact that PLR time to minimum and amplitude are strongly constrained by stimulus properties (intensity, spectrum, duration) and by the differential contribution of photoreceptors (a fast rod/cone component versus a more sustained component involving ipRGCs/melanopsin), which cannot be reduced to background arousal (Pan et al., 2022; Gooley et al., 2012; McDougal and Gamlin, 2010; Adhikari et al., 2016). Finally, the lack of association between hippus frequency and PLR kinematics aligns with work showing robust pupil-respiration coupling at rest but attenuation during tasks, a signature of a state marker rather than a determinant of reflex kinematics (Joshi and Gold, 2020; Kluger et al., 2024). In addition, it is now well established that the PLR can be modulated by attention, further supporting the value of distinguishing kinematics parameters, amplitude, and stimulation context when interpreting links with resting indices (Binda and Gamlin, 2017; Binda et al., 2013).

Iris mechanics appears to be a cross-context determinant of interindividual differences. The PLR baseline diameter correlates with the hippus baseline and with PLR constriction amplitude. Similarly, the hippus baseline is linked to hippus amplitude and to constriction amplitude, suggesting a shared peripheral constraint expressed both in baseline levels and in response amplitudes. These findings are consistent with the view that pupillary dynamics depend not only on autonomic loops, but also on biomechanical properties (elasticity, architecture, innervation) that determine the dynamic range for constriction/dilation and can affect measurements (Strauch and Naber, 2022; Safa et al., 2022). Moreover, the link between constriction amplitude and time to minimum corresponds to the expected mechanical trade-off (a larger response being associated with a longer time to minimum), which has already been described in classic work on interindividual PLR variability (Kelbsch et al., 2019; Bremner, 2001). Conversely, maximal dilation amplitude to faces does not align with PLR kinematics, reinforcing the distinction between phasic social reactivity and PLR dynamics. Finally, iris physiology and the literature on light transmission suggest that differences in pigmentation and retinal illumination may impose shared constraints on baselines and amplitudes (including as a function of eye colour). This is compatible with the idea that light entry depends on pupil diameter particularly in dark irises, and that an iris-colour effect on the PLR is measurable (Strauch and Naber, 2022; Kardon et al., 2013; Bergamin et al., 1998).

Clustering highlights three pupillary profiles: a high-tone/fast profile (high baseline, short time to minimum, high constriction velocity), a hyporeactive profile (low tone, small amplitudes in both the PLR and face conditions), and a slow/hyper-dilated profile (long time to minimum, slow velocity, large facial dilation). These profiles are clearly distinguishable within the sample and are compatible with the LC–NE "adaptive gain" framework, which proposes that an intermediate tonic mode supports efficient phasic responses, whereas tonic levels that are too low or too high are associated with under-engagement or increased variability (Aston-Jones and Cohen, 2005).

Consistent with the adaptive-gain framework, baseline pupil size has been linked to the exploitation-exploration trade-off. Tonically larger pupils predict a shift toward exploratory choices, while tonically smaller pupils predict exploitation choices (Jepma and Nieuwenhuis, 2011). In addition, recent work relates the pupil to the fidelity of cortical representations, suggesting that a high but efficient tonic state can be accompanied by better coding (high-tone/fast) (Geurts et al., 2024). The hyporeactive profile is compatible with autonomic under-engagement, whereas the slow/hyper-dilated profile is compatible with the co-occurrence of slower photomotor kinematics and strong phasic mobilisation by dynamic social stimuli, as already described when social salience and facial motion are high (Ricou et al., 2024; Kret et al., 2013; Bogdanova et al., 2022). To further probe the contribution of state factors, we tested whether daytime recording period was associated with cluster membership, but found no evidence for such an effect. While this suggests that the observed pupillary profiles are unlikely to be primarily driven by diurnal influences, other unmeasured state factors (e.g., sleepiness, recent light exposure, caffeine or other substance intake) may still have influenced pupil dynamics and, consequently, cluster assignment (Jolkovsky et al., 2022; Abokyi et al., 2017). Nevertheless, these findings remain consistent with the possibility that these profiles partly reflect stable individual differences in attentional functioning and LC-NE arousal regulation (tonic baseline and phasic responsivity) (Joshi and Gold, 2020; Robison et al., 2023). In healthy samples, tonic pupil measures have been linked to sustained-attention lapses (van den Brink et al., 2016; Unsworth et al., 2020), and pupil dynamics have also been shown to track off-task states and mind-wandering episodes (Pelagatti et al., 2020).

Finally, the distribution of profiles by sex and eye colour is consistent with literature showing that anatomical and optical factors (including pigmentation) can influence baseline and PLR, even though findings are heterogeneous depending on lighting conditions and measurement methods (Kardon et al., 2013; Bergamin et al., 1998; Tekin et al., 2018; Zheng et al., 2016; Bradley et al., 2010). This variability reinforces the need for strict standardisation of luminance and colour spectrum. Several studies show that the expression of arousal and emotion-related effects depends strongly on illuminance level, with effects often more pronounced at low-to-moderate luminance and attenuated when luminance is high (Pan et al., 2022; Cherng et al., 2020).

This three-axis reading - central tonic, autonomic kinematics, and peripheral contractibility - also helps interpret our negative results. The absence of an inverted-U relationship (Yerkes–Dodson / "adaptive gain") (Aston-Jones and Cohen, 2005) may reflect limited tonic variance in our sample (young adults, stable lighting conditions, brief tasks) and an analysis time window focused on early phasic responses, reducing the likelihood of observing a broad arousal gradient. It is also compatible with the idea that measured pupillary dynamics reflect a compromise between central state, autonomic gain, and peripheral constraints on amplitude capacity: the latter two levels may attenuate or mask centrally driven non-monotonic relationships when iris biomechanics and effective retinal illumination are not finely characterised (Safa et al., 2022; Chen and Kardon, 2013). In this context, stricter control of luminance, together with quantification of iris biomechanical parameters, would be necessary to test more directly the hypothesis of an inverted-U-shaped relationship with central arousal.

Our sample is young and relatively homogeneous. This restriction limits generalisation to other age groups, in which the pupil and its responses (baselines, amplitudes, and kinematics) become more variable (Tekin et al., 2018; Fotiou et al., 2007). Conversely, this homogeneity strengthens mechanistic interpretation within the proposed framework by reducing age-related variance (Kiel et al., 2022) and facilitating the dissociation between the central tonic axis, the autonomic kinetic axis, and the peripheral contractile axis. Broadening the age range will make it possible to test whether the observed phenotypes are maintained and whether their distribution and characteristics change. The facial stimuli are short and not very varied, limiting exploration of the affective and social diversity as described in a broader paradigm (Ricou et al., 2024). However, the short exposure helps minimise habituation and target the early phasic component, which is useful for distinguishing socio-affective reactivity from reflexive and peripheral constraints (Bradley et al., 2008; Snowden et al., 2016). Finally, we did not quantify iris biomechanics (thickness, local elasticity, texture), nor pigmentation

using objective measures. Yet several results suggest that the limiting factor for phasic expression may be peripheral: coherence between hippus baseline, and PLR constriction amplitude; the amplitude and time to minimum association; and modulation by eye colour through the cluster distribution. These elements are consistent with work showing that changes in pupil size are accompanied by radial deformations of the iris (Strauch and Naber, 2022) and that pigmentation modulates effective retinal illumination (Strauch and Naber, 2022; Kardon et al., 2013). Measuring these parameters would help attribute variance more precisely to the peripheral contractile axis (amplitude capacity/optical constraints) and interpret the observed multivariate profiles more finely. It would also be valuable to complement this approach with pupil-HRV coupling to better dissociate vagal and sympathetic components (Alshanskaia et al., 2024), with EEG to index local desynchronisation associated with arousal (Geurts et al., 2024), and with resting-state fMRI to identify networks linked to pupillary fluctuations (DiNuzzo et al., 2019). Taken together, these measures should consolidate the three-axis architecture.

These findings have several implications for the interpretation and design of pupillometry studies. First, they suggest that pupillary parameters should not be interpreted as interchangeable markers of a single physiological mechanism. Baseline diameter, PLR kinematics, hippus characteristics, and face-evoked dilation appear to capture partially distinct components of pupil control. Therefore, study designs should carefully consider which pupil parameter is most appropriate for the mechanism of interest. Second, the identified pupil profiles suggest that inter-individual variability may be informative rather than simply treated as noise. A given participant may show a specific combination of tonic pupil level, PLR kinematics, and stimulus-evoked reactivity, which could influence how their pupil responses are interpreted across tasks. These profiles do not imply that participants should be excluded from pupillometry studies, but they suggest that individual pupil characteristics should be documented and, when possible, integrated into statistical models. Finally, although these profiles may be useful for characterising individual differences in pupil control, they should not be considered diagnostic categories. Their potential use for individual assessment, screening, or clinical purposes will require replication in larger and independent samples, longitudinal stability analyses, and validation against clinical measures.

Overall, our results show that pupillary dynamics emerge from the interaction between three complementary levels: a central tonic arousal axis, an autonomic kinematics axis governing PLR timing, and a peripheral contractile axis linked to iris biomechanics. Notably, the clustering results underscore inter-individual variability in how these three levels combine within a given person, consistent with pupil signals arising from partially separable brain networks whose relative contribution may differ across individuals and contexts. Baseline diameter appears to be a common denominator across contexts: it covaries with hippus and predicts PLR constriction amplitude, and is also reflected in the baseline levels observed during face processing. Hippus oscillations provide a non-invasive index of state: their baseline tracks tonic baseline variations, whereas their amplitude characteristics remain compatible with peripheral constraints, helping to separate global state from mechanical limits. Finally, the absence of a link between hippus frequency and PLR kinematics, together with the dissociation between social reactivity and PLR temporal parameters, reinforces the idea that face-evoked responses cannot be reduced either to background tone or to the PLR loop. Ultimately, approaches combining pupillometry, autonomic measures, neuroimaging, and pharmacology will help clarify the relative contribution of these three axes and test the biomarker value of baseline metrics, PLR kinematics parameters, and hippus characteristics in paradigms integrating PLR and face perception.

CRediT authorship contribution statement

Vivien Rabadan: Writing – original draft, Visualization, Validation, Software, Methodology, Investigation, Funding acquisition, Formal analysis, Data curation, Conceptualization. **Camille Ricou:** Writing – review & editing, Validation, Software, Methodology, Investigation, Formal analysis, Data curation. **Yassine Mofid:** Writing – review & editing, Software, Methodology. **Nadia Aguillon-Hernandez:** Writing – review & editing, Validation, Supervision, Project administration, Funding acquisition, Conceptualization. **Claire Wardak:** Writing – review & editing, Validation, Supervision, Project administration, Funding acquisition, Conceptualization.

Funding sources

VR PhD fellowship is funded by Fondation de France (Allocation jeunes chercheurs en ophtalmologie et neuro-ophtalmologie 2022, 2025), FEANS (Fondation Européenne pour l'Avancement des Neurosciences) and FHU-Exac-t (EXcellence Center for Autism – Tours). CR PhD fellowship was funded by the ANR (ANR-21-CE17-0045-01). The research was funded in part by FHU-Exac-t (EXcellence Center for Autism – Tours) and by l'Agence Nationale de la Recherche (ANR; ANR-21-CE17-0045). For the purpose of open access, the author has applied a CC-BY public copyright licence to any Author Accepted Manuscript (AAM) version arising from this submission.

Declaration of competing interest

The authors declared they have no competing or potential conflicts of interest.

Data availability

Data will be made available on request.

References

Abokyi, S., Owusu-Mensah, J., Osei, K.A., 2017. Caffeine intake is associated with pupil dilation and enhanced accommodation. Eye 31, 615–619.
Adhikari, P., Feigl, B., Zele, A.J., 2016. Rhodopsin and Melanopsin contributions to the early Redilation phase of the post-illumination pupil response (PIPR). PLoS One 11, e0161175.
Aguillon-Hernandez, N., et al., 2020. The pupil: a window on social automatic processing in autism spectrum disorder children. J. Child Psychol. Psychiatry 61, 768–778.
Alshanskaia, E.I., Portnova, G.V., Liaukovich, K., Martynova, O.V., 2024. Pupillometry and autonomic nervous system responses to cognitive load and false feedback: an unsupervised machine learning approach. Front. Neurosci. 18, 1445697.
Aston-Jones, G., Cohen, J.D., 2005. Adaptive gain and the role of the locus coeruleus-norepinephrine system in optimal performance. J. Comp. Neurol. 493, 99–110.
Barbur, J.L., Harlow, A.J., Sahraie, A., 1992. Pupillary responses to stimulus structure, colour and movement. Ophthalmic Physiol. Opt. 12, 137–141.
Benarroch, E.E., 1993. The central autonomic network: functional organization, dysfunction, and perspective. Mayo Clin. Proc. 68, 988–1001.
Bergamin, O., Schoetzau, A., Sugimoto, K., Zulauf, M., 1998. The influence of iris color on the pupillary light reflex. Graefes Arch. Clin. Exp. Ophthalmol. Albrecht Von Graefes Arch. Klin. Exp. Ophthalmol. 236, 567–570.
Berridge, C.W., Schmeichel, B.E., España, R.A., 2012. Noradrenergic modulation of wakefulness/arousal. Sleep Med. Rev. 16, 187–197.
Binda, P., Gamlin, P.D., 2017. Renewed attention on the pupil light reflex. Trends Neurosci. 40, 455–457.
Binda, P., Pereverzeva, M., Murray, S.O., 2013. Attention to bright surfaces enhances the pupillary light reflex. J. Neurosci. 33, 2199–2204.
Bogdanova, O.V., Bogdanov, V.B., Miller, L.E., Hadj-Bouziane, F., 2022. Simulated proximity enhances perceptual and physiological responses to emotional facial expressions. Sci. Rep. 12, 109.
Bolar, K., 2019. STAT: Interactive Document for Working with Basic Statistical Analysis.
Bradley, M.M., Miccoli, L., Escrig, M.A., Lang, P.J., 2008. The pupil as a measure of emotional arousal and autonomic activation. Psychophysiology 45, 602–607.
Bradley, J.C., et al., 2010. The effect of gender and iris color on the dark-adapted pupil diameter. J. Ocul. Pharmacol. Ther. 26, 335–340.
Bremner, F., 2001. The pupil: anatomy, physiology, and clinical applications: by Irene E. Loewenfeld. 1999. Oxford: Butterworth-Heinemann. Price pound180. Pp. 2278. ISBN 0-750-67143-2. Brain 124, 1881–1883.
Breton-Provencher, V., Sur, M., 2019. Active control of arousal by a locus coeruleus GABAergic circuit. Nat. Neurosci. 22, 218–228.
Breton-Provencher, V., Drummond, G.T., Sur, M., 2021. Locus Coeruleus norepinephrine in learned behavior: anatomical modularity and spatiotemporal integration in targets. Front. Neural Circuits 15, 638007.

van den Brink, R.L., Murphy, P.R., Nieuwenhuis, S., 2016. Pupil diameter tracks lapses of attention. PLoS One 11, e0165274.
Bufo, M.R., et al., 2022. Autonomic tone in children and adults: pupillary, electrodermal and cardiac activity at rest. Int. J. Psychophysiol. 180, 68–78.
Campbell, F.W., Green, D.G., 1965. Optical and retinal factors affecting visual resolution. J. Physiol. 181, 576–593.
Carey, S., 1992. Becoming a face expert. Philos. Trans. R. Soc. Lond. Ser. B Biol. Sci. 335, 95–102 discussion 102-103.
Charman, W.N., 2017. Correcting presbyopia: the problem of pupil size. Ophthalmic Physiol. Opt. 37, 1–6.
Chen, Y., Kardon, R.H., 2013. Studying the effect of iris mechanics on the pupillary light reflex using brimonidine-induced anisocoria. Invest. Ophthalmol. Vis. Sci. 54, 2951–2958.
Cherng, Y.-G., Baird, T., Chen, J.-T., Wang, C.-A., 2020. Background luminance effects on pupil size associated with emotion and saccade preparation. Sci. Rep. 10, 15718.
Cortez, M.M., Rea, N.A., Hunter, L.A., Digre, K.B., Brennan, K.C., 2017. Altered pupillary light response scales with disease severity in migrainous photophobia. Cephalalgia Int. J. Headache 37, 801–811.
Critchley, H.D., 2005. Neural mechanisms of autonomic, affective, and cognitive integration. J. Comp. Neurol. 493, 154–166.
Dahl, M.J., Mather, M., Werkle-Bergner, M., 2022. Noradrenergic modulation of rhythmic neural activity shapes selective attention. Trends Cogn. Sci. 26, 38–52.
Dalmaijer, E.S., Nord, C.L., Astle, D.E., 2022. Statistical power for cluster analysis. BMC Bioinform. 23, 205.
DiNuzzo, M., et al., 2019. Brain networks underlying eye's pupil dynamics. Front. Neurosci. 13, 965.
Ducasse, A., 2004. Anatomie et physiologie de l'iris. EMC - Ophtalmol. 1, 1–7.
Fotiou, D.F., et al., 2007. Effect of age on pupillary light reflex: evaluation of pupil mobility for clinical practice and research. Electromyogr. Clin. Neurophysiol. 47, 11–22.
Fox, J., et al., 2026. car: Companion to Applied Regression.
Gamlin, P.D., Zhang, H., Harlow, A., Barbur, J.L., 1998. Pupil responses to stimulus color, structure and light flux increments in the rhesus monkey. Vis. Res. 38, 3353–3358.
Geurts, L.S., Ling, S., Jehee, J.F.M., 2024. Pupil-linked arousal modulates precision of stimulus representation in cortex. J. Neurosci. 44, e1522232024.
Gooley, J.J., et al., 2012. Melanopsin and rod-cone photoreceptors play different roles in mediating pupillary light responses during exposure to continuous light in humans. J. Neurosci. 32, 14242–14253.
Hu, X., Hisakata, R., Kaneko, H., 2019. Effects of spatial frequency and attention on pupillary response. J. Opt. Soc. Am. A Opt. Image Sci. Vis. 36, 1699–1708.
Jepma, M., Nieuwenhuis, S., 2011. Pupil diameter predicts changes in the exploration-exploitation trade-off: evidence for the adaptive gain theory. J. Cogn. Neurosci. 23, 1587–1596.
Jolkovsky, E.L., et al., 2022. Impact of acute intoxication on quantitative pupillometry assessment in the emergency department. J. Am. Coll. Emerg. Physicians Open 3, e12825.
Joshi, S., Gold, J.I., 2020. Pupil size as a window on neural substrates of cognition. Trends Cogn. Sci. 24, 466–480.
Joshi, S., Li, Y., Kalwani, R.M., Gold, J.I., 2016. Relationships between pupil diameter and neuronal activity in the Locus Coeruleus, Colliculi, and Cingulate Cortex. Neuron 89, 221–234.
Joyce, D.S., Feigl, B., Cao, D., Zele, A.J., 2015. Temporal characteristics of melanopsin inputs to the human pupil light reflex. Vis. Res. 107, 58–66.
Kane, G.A., et al., 2017. Increased locus coeruleus tonic activity causes disengagement from a patch-foraging task. Cogn. Affect. Behav. Neurosci. 17, 1073–1083.
Kang, O., Wheatley, T., 2015. Pupil dilation patterns reflect the contents of consciousness. Conscious. Cogn. 35, 128–135.
Kardon, R.H., Hong, S., Kawasaki, A., 2013. Entrance pupil size predicts retinal illumination in darkly pigmented eyes, but not lightly pigmented eyes. Invest. Ophthalmol. Vis. Sci. 54, 5559–5567.
Kelbsch, C., et al., 2019. Standards in pupillography. Front. Neurol. 10, 129.
Kiel, M., et al., 2022. Distribution of pupil size and associated factors: results from the population-based Gutenberg health study. J. Ophthalmol. 2022, 9520512.
Kluger, D.S., Gross, J., Keitel, C., 2024. A dynamic link between respiration and arousal. J. Neurosci. 44, e1173242024.
Kret, M.E., Roelofs, K., Stekelenburg, J.J., de Gelder, B., 2013. Emotional signals from faces, bodies and scenes influence observers' face expressions, fixations and pupil-size. Front. Hum. Neurosci. 7, 810.
Laeng, B., Sirois, S., Gredebäck, G., 2012. Pupillometry: a window to the preconscious? Perspect. Psychol. Sci. J. Assoc. Psychol. Sci. 7, 18–27.
Larsen, R.S., Waters, J., 2018. Neuromodulatory correlates of pupil dilation. Front. Neural Circuits 12, 21.
Li, Q., et al., 2021. Measurement of iris thickness at different regions in healthy Chinese adults. J. Ophthalmol. 2021, 2653564.
Lloyd, B., de Voogd, L.D., Mäki-Marttunen, V., Nieuwenhuis, S., 2023. Pupil size reflects activation of subcortical ascending arousal system nuclei during rest. eLife 12, e84822.
Maechler, M., et al., 2026. cluster: 'Finding Groups in Data': Cluster Analysis Extended Rousseeuw et al.
Manion, G.N., Stokkermans, T.J., 2025. The effect of pupil size on visual resolution. In: StatPearls. StatPearls Publishing, Treasure Island (FL).
Marumo, C., Nakano, T., 2021. Early phase of pupil dilation is mediated by the peripheral parasympathetic pathway. J. Neurophysiol. 126, 2130–2137.
McCorry, L.K., 2007. Physiology of the autonomic nervous system. Am. J. Pharm. Educ. 71, 78.
McDougal, D.H., Gamlin, P.D., 2010. The influence of intrinsically-photosensitive retinal ganglion cells on the spectral sensitivity and response dynamics of the human pupillary light reflex. Vis. Res. 50, 72–87.
McDougal, D.H., Gamlin, P.D., 2015. Autonomic control of the eye. Compr. Physiol. 5, 439–473.
Megemont, M., et al., 2024. Simultaneous recordings of pupil size variation and locus coeruleus activity in mice. STAR Protoc. 5, 102785.
Murphy, P.R., Robertson, I.H., Balsters, J.H., O'connell, R.G., 2011. Pupillometry and P3 index the locus coeruleus-noradrenergic arousal function in humans. Psychophysiology 48, 1532–1543.
Murphy, P.R., Vandekerckhove, J., Nieuwenhuis, S., 2014. Pupil-linked arousal determines variability in perceptual decision making. PLoS Comput. Biol. 10, e1003854.
Murrell, P., 2020. RGraphics: Data and Functions from the Book R Graphics, Third Edition.
Pan, J., Klímová, M., McGuire, J.T., Ling, S., 2022. Arousal-based pupil modulation is dictated by luminance. Sci. Rep. 12, 1390.
Pelagatti, C., Binda, P., Vannucci, M., 2020. A closer look at the timecourse of mind wandering: pupillary responses and behaviour. PLoS One 15, e0226792.
Rabadan, V., et al., 2026. From low-level to high-level factors' influence on pupil hippus. J. Neurophysiol. 135, 51–64.
Reimer, J., et al., 2016. Pupil fluctuations track rapid changes in adrenergic and cholinergic activity in cortex. Nat. Commun. 7, 13289.
Ricou, C., Rabadan, V., Mofid, Y., Aguillon-Hernandez, N., Wardak, C., 2024. Pupil dilation reflects the social and motion content of faces. Soc. Cogn. Affect. Neurosci. **19**, nsae055.
Ricou, C., et al., 2026. Invariant response to faces in ASD: unexpected trajectory of oculo-pupillometric biomarkers from childhood to adulthood. Brain Res. 1871, 150070.
Robison, M.K., et al., 2023. Testing locus coeruleus-norepinephrine accounts of working memory, attention control, and fluid intelligence. Cogn. Affect. Behav. Neurosci. 23, 1014–1058.
Safa, B.N., Bahrani Fard, M.R., Ethier, C.R., 2022. In vivo biomechanical assessment of iridial deformations and muscle contractions in human eyes. J. R. Soc. Interface 19, 20220108.
Sara, S.J., 2009. The locus coeruleus and noradrenergic modulation of cognition. Nat. Rev. Neurosci. 10, 211–223.
Sara, S.J., Bouret, S., 2012. Orienting and reorienting: the locus coeruleus mediates cognition through arousal. Neuron 76, 130–141.
Schneider, M., et al., 2016. Spontaneous pupil dilations during the resting state are associated with activation of the salience network. NeuroImage 139, 189–201.
Snowden, R.J., et al., 2016. The pupil's response to affective pictures: role of image duration, habituation, and viewing mode. Psychophysiology 53, 1217–1223.
Sobczak, F., Pais-Roldán, P., Takahashi, K., Yu, X., 2021. Decoding the brain state-dependent relationship between pupil dynamics and resting state fMRI signal fluctuation. eLife 10, e68980.
Strauch, C., Naber, M., 2022. Irissometry: effects of pupil size on Iris elasticity measured with video-based feature tracking. Invest. Ophthalmol. Vis. Sci. 63, 20.
Szabadi, E., 2012. Modulation of physiological reflexes by pain: role of the locus coeruleus. Front. Integr. Neurosci. 6, 94.
Szabadi, E., 2018. Functional organization of the sympathetic pathways controlling the pupil: light-inhibited and light-stimulated pathways. Front. Neurol. 9, 1069.
Tekin, K., et al., 2018. Static and dynamic pupillometry data of healthy individuals. Clin. Exp. Optom. 101, 659–665.
Thayer, J.F., Lane, R.D., 2000. A model of neurovisceral integration in emotion regulation and dysregulation. J. Affect. Disord. 61, 201–216.
Thayer, J.F., Hansen, A.L., Saus-Rose, E., Johnsen, B.H., 2009. Heart rate variability, prefrontal neural function, and cognitive performance: the neurovisceral integration perspective on self-regulation, adaptation, and health. Ann. Behav. Med. 37, 141–153.
Unsworth, N., Miller, A.L., Robison, M.K., 2020. Individual differences in lapses of sustained attention: Ocolumetric indicators of intrinsic alertness. J. Exp. Psychol. Hum. Percept. Perform. 46, 569–592.
Van Egroo, M., Koshmanova, E., Vandewalle, G., Jacobs, H.I.L., 2022. Importance of the locus coeruleus-norepinephrine system in sleep-wake regulation: implications for aging and Alzheimer's disease. Sleep Med. Rev. 62, 101592.
Wei, T., et al., 2024. corrplot: Visualization of a Correlation Matrix.
Wickham, H., et al., 2026. ggplot2: Create Elegant Data Visualisations Using the Grammar of Graphics.
Yamazaki, Y., et al., 2023. A possible contribution of the Locus coeruleus to arousal enhancement with mild exercise: evidence from pupillometry and neuromelanin imaging. Cereb. Cortex Commun. 4, tgad010.
Yang, H., Bari, B.A., Cohen, J.Y., O'Connor, D.H., 2021. Locus coeruleus spiking differently correlates with S1 cortex activity and pupil diameter in a tactile detection task. eLife 10, e64327.
Yellin, D., Berkovich-Ohana, A., Malach, R., 2015. Coupling between pupil fluctuations and resting-state fMRI uncovers a slow build-up of antagonistic responses in the human cortex. NeuroImage 106, 414–427.
Zerbi, V., et al., 2019. Rapid reconfiguration of the functional connectome after Chemogenetic Locus Coeruleus activation. Neuron 103, 702–718.e5.
Zheng, C., et al., 2016. Determinants of pupil diameters and pupil dynamics in an adult Chinese population. Graefes Arch. Clin. Exp. Ophthalmol. 254, 929–936.